"Look deep into nature, and then you will understand everything better."

— Albert Einstein

CHAPTER 1

INTRODUCTION

In this chapter, we provide a general introduction to elementary particle physics, including a brief discussion of the fundamental building blocks of matter, quantum chromodynamics (QCD), deep inelastic scattering (DIS), parton distribution functions (PDFs), nucleon structure functions, and parton evolution equations. This chapter provides a brief description of small-x physics and nonlinear processes such as gluon recombination and saturation. The importance of nonlinear parton evolution equations is explained in this chapter.

1.1 Fundamental Building Blocks of Matter

Understanding the origin of matter at the elementary level has been one of the primary goals of particle physics research. Matter makes up everything that surrounds us, including us and the whole universe. However, questions come up: *What constitutes the matter? What are the basic components or elements that make up matter?* The desire to understand the fundamental building blocks of matter dates back to ancient times. Philosophers of antiquity conjectured that the four sets of basic elements—earth, water, air, and fire—were the main components of nature. The

fifth element was later included in ancient Greek and traditional Indian philosophy, respectively, as "aether" (a material medium that spreads all across space) and "akasha" [1]. Until the renowned chemist Robert Boyle developed a new concept of elements at the start of the modern era, these five elements were believed to be the fundamental building blocks of nature. He defines an element as a basic, distinct substance that is incapable of being further broken down into simpler compounds. In 1809, around a century later, British chemist John Delton published the famous atomic theory describing matter in the form of the smallest particles called the "atom". In consequence, Russian chemist Dmitri Mendeleev attempted to organize all elements by atomic weight into a table, presently known as the periodic table.

For a long time, it was thought that atoms were the ultimate particles that matter is formed of and could not be further divided. However, investigations undertaken in the late nineteenth and early twentieth centuries indicated that the atom is not the ultimate particle. The persistent efforts of scientists resulted in the discovery of subatomic particles. In 1897, Joseph John Thomson discovered the electron, the first-ever subatomic particle. Ernest Rutherford's renowned gold foil experiment in 1911 resulted in the identification of the proton. This implies that atoms are made up of a positively charged core termed the nucleus orbited by negatively charged electrons. In 1932, scientists hypothesised the existence of a neutral particle in an atom's nucleus, following Ernest Rutherford's initial proposal in 1920. James Chadwick discovered the neutal particle, today known as the neutron, in 1932. Contemporary advancements in atomic structure and quantum physics have resulted in the identification of numerous additional basic particles. The finding of subatomic particles has facilitated several subsequent breakthroughs and discoveries.

By the 1960s, a large number of new particles had been discovered, such as proton and neutron, which are referred to as hadrons. Nonetheless, it was reasonable to acknowledge that the hadrons were strongly bound composite objects of some

further small entities rather than true fundamental particles. In 1964, Murray Gell-Mann and George Zweig independently proposed the idea of the quark model, which proposed the existence of small entities inside hadrons [2, 3]. They coined these small entities as quarks, which are responsible for the composite structure of hadrons. Each hadron, in their suggested theory, was made up of either a quark and anti-quark pair (mesons), or three quarks (baryons). Subsequently, in 1968, an electron-proton deep inelastic scattering (DIS) experiment at the Stanford Linear Accelerator Center (SLAC) confirmed the existence of quarks within the proton. Soon after, in 1969, Richard Feynman came up with a model of hadrons and proposed the parton model. According to his model, the hadrons—which he called "partons"—were composite objects of a more fundamental particle. [4]. Later, based on experimental observations and the validation of the quark model, partons were identified as the same objects as what we know today as quarks and gluons.

In the twenty-first century, our knowledge of the underlying components of matter has progressed from atomic models to a clearer and comprehensive representation of these components in terms of elementary particles. When we refer to elementary particles, we mean those that are point-like or structureless and lack any recognised structure. They are unresolvable into two or more components. The branch of natural science known as particle physics focuses on the fundamental constituents of matter, known as elementary particles, and their interactions with one another. Significant advancements in particle physics over the past century have fundamentally altered our comprehension of basic queries concerning the building blocks of matter. Physicists have attempted to delve deep inside the atom to discover the constituent particles, quarks, and gluons within the nucleon. The current state of particle physics research shows physicists' most ambitious and organized endeavor to address questions regarding the fundamental building blocks of matter.

The standard model (SM) [5–8] of particle physics is the most effective theory

that we currently have and is well tested at current accelerator facilities, describing all the known elementary particles and their interactions among them. This theory was progressively formulated by physicists globally during the second part of the 20th century, with the current version established in the mid-1970s after experimental confirmation of quark existence. This has been further corroborated by the discovery of particles such as the W and Z bosons [9], the top quark [10], the tau neutrino [11], and, most recently, the Higgs boson at CERN's Large Hadron Collider (LHC) in 2012 [12]. The Standard Model asserts that quarks, leptons, and their antiparticles constitute the fundamental constituents of matter in the universe. Six distinct varieties of quarks and leptons exist, with force-carrier particles facilitating their interactions. Ordinary matter is made up of fermions, such as leptons and quarks, while force-carrying particles are bosons. All of these elementary particles are categorized into three generations in the Standard Model.

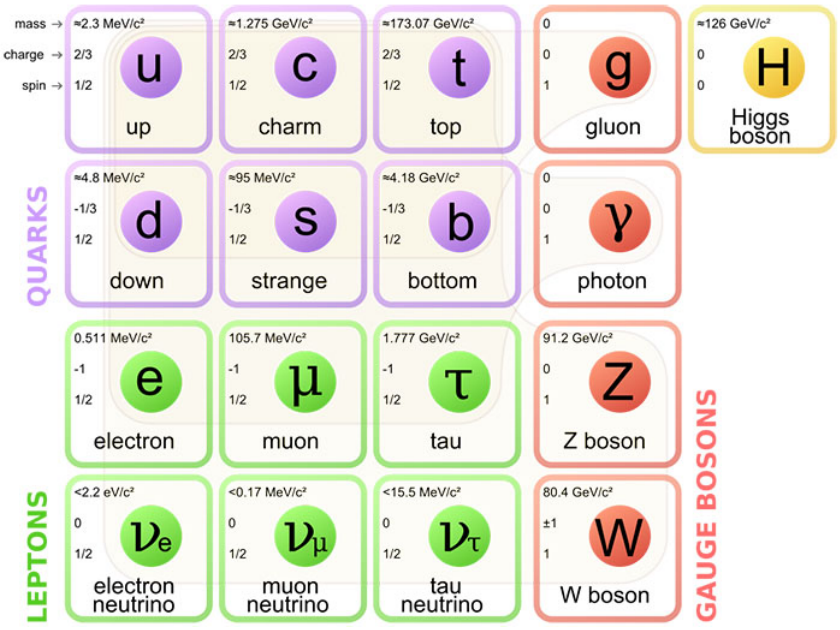

Figure 1.1: Elementary particles of the standard model

Nature is regulated by four fundamental forces: the strong nuclear force, the electromagnetic force, the weak nuclear force, and gravitational force. These forces

delineate all interactions inside the cosmos. The Standard Model encompasses three of the four fundamental forces. It encompasses the electromagnetic, strong, and weak forces, together with their corresponding carrier particles, and accurately delineates the interactions between them. However, the SM does not include gravity, which is the most intuitive and well-known aspect in our daily lives. All of these fundamental forces operate in various ranges and at varying strengths. Both gravity and the electromagnetic force act across an unlimited range, but the electromagnetic force is several orders of magnitude stronger than gravity. Strong and weak forces are only effective over extremely short distances and dominate at the subatomic level. All fundamental forces have their own force carriers, and particles serve as mediators between interactions. It has been suggested that gravity is transmitted by a hypothetical particle known as the graviton that has yet to be discovered. According to some theorists, the LHC's high-energy experiments could produce gravitons, which would rapidly escape into extra dimensions.

Quantum electrodynamics (QED), a quantum field theory, provides a mathematical account of the interactions between the electromagnetic field and matter particles, as well as between charged particles. The electromagnetic interactions among electrically charged particles are exchanged via spin 1 gauge bosons called photons, which are uncharged. The sun is powered by nuclear fusion and the disintegration of unstable subatomic particles, both of which are caused by the weak interaction. The weak interaction, involving two mediator particles, Z^0 and $W^{\pm}$, influences all SM fermions, including the Higgs boson. They are known as intermediate vector bosons. Neutrinos are particularly challenging to study since they are the sole particles that only experience weak interaction. At higher energies, the electro-weak theory (EWT) of Glashow, Salam, and Weinberg integrates the weak and electromagnetic forces into one, providing the finest understanding of the weak interaction [6–8].

Hadrons are composed of quarks and gluons which have a color charge and hence

interact strongly. The mathematical description of strong interactions is provided by Quantum chromodynamics (QCD), an area of quantum field theory, which will be studied in the following section. Quarks' strong interactions are exchanged by massless gluons with spin 1, similar to photons in QED. However, gluons in QCD can interact with themselves since they have color charge, unlike photos in QED. This self-interaction of gluons makes QCD more interesting and challenging to explain than QED.

1.2 Quantum Chromodynamics: The Theory of Strong Interactions

The strongest force in nature, the strong force, binds quarks and antiquarks together inside hadrons. It is carried by its own force-carrying particle, gluon. In theoretical physics, this force is described by quantum chromodynamics (QCD), a quantum field theory analogous to quantum electrodynamics (QED), which delineates the strong interaction among quarks and gluons that generates hadrons (mesons and baryons). The lagrangian of the theory is given by

$$\mathcal{L}_{QCD} = \sum_q \left(\bar{\psi}_{qi} i\gamma^\mu \left[\delta_{ij}\partial_\mu + ig\left(G^\alpha_\mu t_\alpha \right)_{ij} \right] \psi_{qj} - m_q \bar{\psi}_{qi}\psi_{qi} \right) - \frac{1}{4} G^\alpha_{\mu\nu} G^{\mu\nu}_\alpha. \quad (1.1)$$

Here, ψ_i signifies the Dirac spinor for the quark field (with i indicating color), and t_α represents the generators of the $SU(3)$ gauge group (where $\alpha = 1, \ldots, 8$), corresponding to the 3×3 Gell-Mann matrices. The field strength tensor $G^{\mu\nu}_\alpha$ for the gluon field G^α_μ is given by

$$G^{\mu\nu}_\alpha = \partial^\mu G^\nu_\alpha - \partial^\nu G^\mu_\alpha - g f^{\alpha\beta\gamma} G^\mu_\beta G^\nu_\gamma, \quad (1.2)$$

where $g = \sqrt{4\pi\alpha_s}(\hbar = c = 1)$ is the color charge (strong coupling constant), whereas $f^{\alpha\beta\gamma}$ represents the structure constants of the $SU(3)$ gauge group. The extra degree of freedom associated with this gauge group is called color, the strong charge, and it has nothing to do with the common, everyday occurrence of color.

After the discovery of the Δ^{++} baryon, Greenberg proposed the color charge in 1964 to reconcile spin-statistics conflicts in hadron spectroscopy. Three-up quarks with parallel spins are discovered in this baryon, defying the well-known Pauli's exclusion principle. In the 1970s, physicists Heinrich Leutwyler, Murray Gell-Mann, and Harald Fritzsch proposed that color is the source of a strong field, which led to the development of QCD, the theory of strong interactions [13]. They specifically used the general field theory, which was proposed in the 1950s by *Yang and Mills* and states that a force's carrier particles have the ability to radiate other carrier particles. This is different from QED, where the photons carrying the electromagnetic force do not radiate further photons. QCD states that the color charge of each quark is red (R), green (G), or blue (B), and for antiquarks it is antired (Cyan), antigreen (Magenta), and antiblue (Yellow), i.e., $\bar{R}$, $\bar{G}$, $\bar{B}$ [14]. In contrast to photons in QED, gluons in QCD carry a color charge. This important distinction makes QCD a more sophisticated theory than QED. In QCD lagrangian, the gluon field strength tensor includes a non-ablelian term (see Eq. (1.2)) that accounts for self-interaction between color-charged gluons. The schematic representation of basic QCD Feynman diagrams is shown in Figure 1.2.

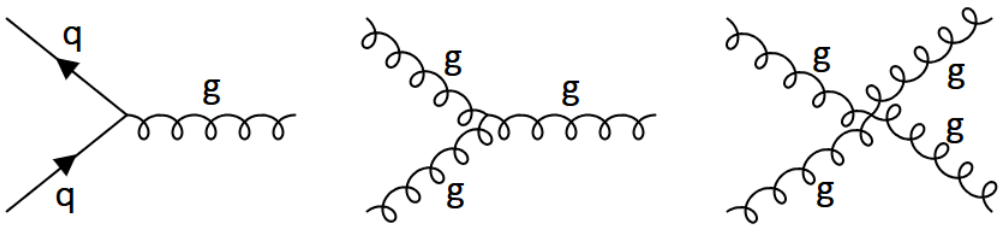

Figure 1.2: Basic QCD Feynman diagrams

Asymptotic freedom and color confinement are two most notable features of QCD [15–17]. The perturbative calculations of QCD are fundamentally grounded on the principle of asymptotic freedom, which indicates that quarks and gluons behave as quasi-free particles at short distances, while the strong interaction strengthens at larger distances. In reality, we do not see free quarks in nature, as they are confined within the composite states of hadrons that are observed experimentally. These unique features of strong interaction, which make QCD interesting, can be understood through the strong coupling constant. The strong coupling constant is an effective measure of how strongly a force holds quarks and gluons inside composite hadrons. This constant ought to depend on the absolute energy scale, and hence it is also referred to as the running coupling constant [18]. Thus, the strong coupling constant is not constant any more; rather, it varies with the energy scale used. The so-called beta function governs the running, which is logarithmic with energy and it can be represented as given by

$$\frac{\partial \alpha_s}{\partial \ln(Q^2)} = \beta(\alpha_s) = -\left(\frac{\alpha_s^2}{4\pi}\right)^2 \sum_{n=0} \left(\frac{\alpha_s^2}{4\pi}\right)^n \beta_n. \tag{1.3}$$

The values of coefficients for one-loop, two-loop, and three-loop are given by

$$\beta_0 = \frac{11}{3}N_c - \frac{4}{3}T_f = 11 - \frac{2}{3}N_f,$$
$$\beta_1 = \frac{34}{3}N_c^2 - \frac{10}{3}N_c N_f - 2C_F N_f = 102 - \frac{38}{3}N_f,$$

and

$$\beta_2 = \frac{2857}{54}N_c^3 + 2C_F^2 T_f - \frac{205}{9}C_F N_c T_f - \frac{1415}{27}N_c^2 T_f + \frac{44}{9}C_F T_f^2 + \frac{158}{27}N_c T_f^2$$
$$= \frac{2857}{2}\frac{6673}{18}N_f + \frac{325}{54}N_f^2.$$

N_c denotes the quantity of colors, whereas N_f signifies the number of active fermion flavors. The color factor for the gauge group $SU(3)$ is denoted as C_f, with $N_f = 4$,

$N_c = 3$, $T_f = \frac{1}{2}N_f$, and $C_f = \frac{N_c^2-1}{2N_c}$. To effectively define the value of the strong coupling, two parameters are typically employed: the renormalization scale (μ_R) and the value of the strong coupling (α_s) at the renormalization scale. This allows one to use Eq. (1.3) to determine its value at any other scale as

$$\alpha_s(Q^2) = \frac{\alpha_s(\mu_R^2)}{1 + \alpha_s(\mu_R^2)\beta_0 \ln(Q^2/\mu_R^2) + \mathcal{O}(\mu_R^2)}. \tag{1.4}$$

The above expression of the running coupling can be recasted with a single parameter Λ_{QCD} replacing the two parameters as

$$\alpha_s(Q^2) = \frac{1}{\beta_0 \ln(Q^2/\Lambda_{QCD}^2)}. \tag{1.5}$$

The confinement scale of QCD, or parameter Λ_{QCD}, was experimentally determined to be $\Lambda_{QCD} \approx 200$ MeV. This in turn suggests that only at an energy scale of 1 GeV or greater are the perturbation calculations applicable. Furthermore, confinement makes it impossible to use perturbation theory to determine the structure of hadrons. Alternatively, the quark and gluon composition of hadrons is determined by parameterizations of the distribution functions derived from deep inelastic scattering studies. These distribution functions serve as crucial in making predictions for further experiments because they are universal.

1.3 Deep Inelastic Scattering

Deep Inelastic Scattering (DIS) [19, 20] is an essential means for investigating the internal composition of hadrons (e.g., nucleons) and comprehending the interaction dynamics of quarks and gluons within these particles. In DIS, high-energy leptons (electron, muon, neutrino, etc.) are directed towards hadron targets (proton, neutron), leading to the formation of various final-state hadrons. The first DIS experiment

was carried out in 1968 at the Stanford Linear Accelerator Centre (SLAC) in the United States, with electrons scattered off proton targets. The results of the SLAC experiment provided the first conclusive evidence for the reality of quarks, which were previously thought to be a mathematical construction. A schematic diagram of the DIS process of scattering a lepton off a hadron is shown in Figure 1.3. In this process, accelerating the lepton to very high energy are allowed to collide with the hadron. The lepton engages with the target hadron through the exchange of a virtual photon throughout the interaction. The virtual photon exchanged by the lepton carries the four momentum Q, the squared of which, i.e., Q^2, is the measure of the resolving power of the process.

DIS experiments pave the groundwork for the discovery and interpretation of novel physics at extremely high energies and high parton densities within hadrons. Many further DIS experiments investigating proton structure were conducted at HERA, after the very first DIS experiment at SLAC in 1968. The Large Hadron Electron Collider (LHeC) [21], a new colliding beam facility to be built at CERN, was proposed recently by physicists. This will enable the particle physics community to perform DIS experiments to enrich the physics made possible by the Large Hadron Collider (LHC). LHeC with a center of mass energy of 1.3 TeV will create a previously unlocked kinematic domain for electron-hadron scattering. The predicted design luminosity for LHeC is $10^{33}\ cm^{-2}s^{-1}$, which is two orders of magnitude higher than that of integrated HERA luminosity. The LHeC facility is expected to explore a wide range of intriguing phenomena.

Deep inelastic scattering (DIS) of leptons (l) on nucleons (N=p,n) involving the exchange of a neutral boson, either a photon (γ^*) or a vector boson Z^0, is termed neutral current (NC) DIS; conversely, if the exchanged particle is a charged boson, $W^{\pm}$, it is designated as charged current (CC) DIS. Figure 1.3 illustrates the kinematics of the Deep Inelastic Scattering (DIS) process using the following four-

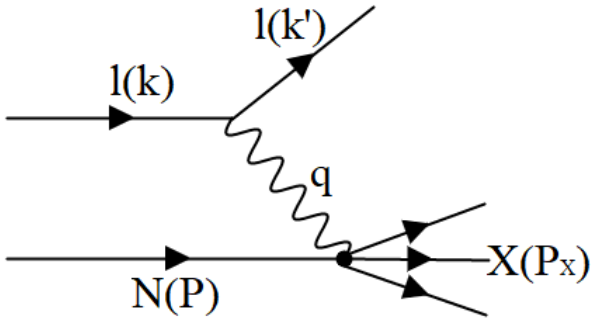

Figure 1.3: Schematic representation of lepton(l)-nucleon(N) deep inelastic scattering process

momentum vectors: k for the initial lepton, k' for the final lepton, P for the target proton, and $q = k - k'$ for the exchanged photon. An inclusive DIS is a measurement that aggregates all final states within the hadronic system. The inclusive DIS process can be explained through the following Lorentz invariant kinematic variables [14]

- $Q^2 = -q^2 = -(k - k')^2$, exchanged four-momentum squared or virtuality of photon, determines the scale of the interaction,
- $x = Q^2/2\nu$, Bjorken's scaling variable, represents the momentum fraction carried by a parton, where $\nu = P.q$ is the energy transferred from the lepton to the proton,
- $y = P.q/P.k$, fraction of energy lost by the electron in the proton rest frame, known as the inelasticity of the scattering process,
- $s = (k + P)^2$, center of mass energy squared, and
- $W^2 = (q + P)^2$, square of the invariant mass of the produced hadronic final state or center of mass energy squared of the photon-proton system.

Two independent variables in DIS process are Q^2 and ν. The approximate relation $Q^2 = xys$ relates the dimensionless variable x to the variables Q^2, y, and s stated above. This relationship indicates that at a specific e-p center of mass energy $\sqrt{s}$,

any two of the variables Q^2, x, and y suffice to characterize the kinematics of the DIS process; typically, Q^2 and x are employed. The kinematic variable W^2 can also be expressed in relation to Q^2 and x as

$$W^2 = M_p^2 + Q^2\Big(\frac{1-x}{x}\Big).$$

The above relation explains that at fixed Q^2, small-x interaction corresponds to a large value of the variable W^2. It also signifies that the terms 'deep' and 'inelastic' correspond to $Q^2 >> M_p^2$ and $W^2 >> M_p^2$, respectively. Thus, the value of the proton mass M_p may be neglected.

1.4 DIS Cross Section and Structure Functions

A crucial component of DIS experiments is the measurement of the scattering cross section. The lepton-proton DIS cross section can be separated out in terms of the electron and proton contributions into leptonic and hadronic parts, which can be expressed as

$$d\sigma \sim L_{\mu\nu}W^{\mu\nu}. \tag{1.6}$$

Here, $L_{\mu\nu}$ denotes the leptonic tensor that characterizes the interaction between the lepton and the exchanged gauge boson, while $W^{\mu\nu}$ signifies the hadronic tensor that encapsulates the strong interaction dynamics in DIS. The leptonic tensor, well known in QED, can be expressed (neglecting the electron mass) as

$$L_{\mu\nu} = 2(k'_\mu k_\nu + k'_\nu k_\mu - (k'.k)g_{\mu\nu}), \tag{1.7}$$

where $g_{\mu\nu}$ represents the metric tensor. The hadronic tensor describing the hadron vertex has the form

$$\begin{aligned} W^{\mu\nu} = &- W_1 g^{\mu\nu} + \frac{W_2}{M_p^2} p^\mu p^\nu - i\epsilon^{\mu\nu\alpha\beta} p_\alpha q_\beta \frac{W_3}{2M_p^2} + q^\mu q^\nu \frac{W_4}{M_p^2} \\ &+ (p^\mu q^\nu + q^\mu p^\nu)\frac{W_5}{M_p^2} + i(p^\mu q^\nu - p^\nu q^\mu)\frac{W_6}{2M_p^2}, \end{aligned} \tag{1.8}$$

where W_i is the Lorentz scalar function of x, and Q^2 characterizes the proton's structure. For the scattering process involving only γ exchange, the parity violating term W_3 and the antisymmetric term W_6 are absent. From the current conservation at the hadronic vertex, we have, $q_\mu W^{\mu\nu} = q_\nu W^{\mu\nu} = 0$, so that

$$W_4 = \left(\frac{p.q}{q^2}\right)^2 W_2 + \frac{M_p^2}{q^2} W_1 \quad \& \quad W_5 = -\frac{p.q}{q^2} W_2.$$

Thus, the hadronic tensor $W^{\mu\nu}$, by assuming it to be symmetric, depends on W_1 and W_2 only and can be expressed as

$$W^{\mu\nu} = -W_1\Big(- g^{\mu\nu} + \frac{q^\mu . q^\nu}{q^2}\Big) + \frac{W_2}{M_p^2}\Big(p^\mu - \frac{p\cdot q}{q^2} q^\mu\Big)\Big(p^\nu - \frac{p\cdot q}{q^2} q^\nu\Big). \tag{1.9}$$

The functions W_1 and W_2 are referred to as structure functions, which can be empirically determined by analyzing the angular dependency of the DIS cross-section given by in [14, 22].

$$\frac{d\sigma^{ep}}{dE' d\Omega} = \frac{\alpha^2}{4E^2 \sin[4](\frac{\theta}{2})}\Big[W_2(x, Q^2)\cos[2](\frac{\theta}{2}) + 2W_1(x, Q^2)\sin[2](\frac{\theta}{2})\Big]. \tag{1.10}$$

Here α denotes the electromagnetic coupling constant. θ is the scattering angle and E, E' are the initial and final electron energies, respectively. It is much more convenient to redefine these structure functions in terms of dimensionless structure

functions F_1 and F_2 as

$$F_1 = M_p W_1(x, Q^2), \tag{1.11a}$$

$$F_2 = \frac{p.q}{M_p} W_2(x, Q^2). \tag{1.11b}$$

The unpolarized double differential DIS cross-section can be expressed in terms of these structure functions in the form

$$\frac{d^2\sigma}{dxdQ^2} = \frac{4\pi\alpha^2}{xQ^4}\Big[xy^2 F_1(x, Q^2) + (1-y)F_2(x, Q^2)\Big]. \tag{1.12}$$

The structure function $F_1(x, Q^2)$ represents the transverse component of the cross-section caused by the transversely polarized virtual photon. The difference between $F_2(x, Q^2)$ and $F_1(x, Q^2)$ provides the pure longitudinal part, given by

$$F_L(x, Q^2) = F_2(x, Q^2) - 2xF_1(x, Q^2). \tag{1.13}$$

Now, the cross-section in terms of the longitudinal structure function can be written as

$$\frac{d^2\sigma}{dxdQ^2} = \frac{2\pi\alpha^2}{xQ^4}\Big[Y_+ F_2(x, Q^2) - y^2 F_L(x, Q^2)\Big], \tag{1.14}$$

where $Y_+ = 1 + (1-y)^2$ is a function of inelasticity y. Structure functions are taken from the measured cross-section in DIS experiments. For convenience, the reduced cross-section can therefore be defined as

$$\sigma_r = F_2(x, Q^2) - \frac{y^2}{Y_+} F_L(x, Q^2). \tag{1.15}$$

In the limit $Q^2 \to \infty$ and fixed x, one can ignore the strong interactions among partons. The proton structure functions can be approximated by an incoherent summation of the partons. Consequently, F_1 and F_2 transform into functions ex-

clusively of the variable x, rendering them independent of Q^2. Bjorken scaling refers to the phenomena of this scaling behavior [23]. The renowned SLAC-MIT experiment on Deep Inelastic Scattering (DIS) [24] demonstrates that the measured DIS cross-section has a near-scaling behavior. In the Bjorken limit, only transversally polarized photons can be absorbed by the quarks in the proton; longitudinally polarized photons cannot be absorbed because of helicity conservation, and as a result, the longitudinal portion of the cross-section disappears. This fact guides to the well-known Callan-Gross relation $2xF_1(x) = F_2(x)$, reflecting the presence of quarks with spin $1/2$ inside the proton.

QCD framework permits partons to interact through gluon exchange by extending the basic quark-parton model. Because of QCD, there is a possibility of processes like $q \to qg$, $g \to gg$, and $g \to q\bar{q}$ that generate the first-order parton interactions in α_s. The resolution of the exchange photon in DIS is proportional to $1/Q^2$. Increasing Q^2 leads to higher parton density. The cross-sectional study demonstrates that the increase occurs predominantly at small x values. Consequently, parton densities in QCD must be represented using an extra scale Q^2. Significant scaling violations are caused by higher order corrections in $\alpha_s(Q^2)$, which cause the parton distribution functions (PDFs) and structure functions to develop a Q^2 dependency beyond the parton model approximation [25]. The proton structure function F_2 was measured extensively in the HERA experiments, H1 and ZEUS [26–29], which also successfully demonstrated the scaling violations as predicted by QCD. The expected scale dependency provides an explicit verification of QCD and enables an exact estimation of $\alpha_s(Q^2)$.

1.5 Parton Distribution Functions

In experiments at different high-energy collider facilities, including HERA, Tevatron, and LHC, the initial-state particles are composite hadrons instead of quarks and gluons, so perturbative QCD calculations involving initial-state hadrons cannot offer a direct evaluation of structure functions. It is necessary to understand the momentum distributions of the partons within colliding hadrons to correlate theoretical QCD calculations with experimental results. The momentum distribution functions of the colliding hadrons are simply referred to as parton distribution functions (PDFs). PDFs are crucial for accurately measuring hadron structure functions, at least at the zeroth order in α_s. In his parton model, Feynman postulated that the proton is made up of more fundamental components called partons, each of which has a momentum fraction x of the proton's total momentum. According to the concept, for each quark flavor i, the structure functions are typically determined by summing the momentum distributions $q_i(x)$ of partons as

$$F_2(x) = 2xF_1(x) = \sum_i e_i^2 x q_i(x), \tag{1.16}$$

where e_i represents the electric charge of a i-type parton, and the sum includes all quark and antiquark flavors. The momentum distribution $q_i(x)$ depicts the probability densities for detecting an individual parton of type i with a momentum fraction x within the proton at resolution scale Q^2.

DIS experiments have demonstrated that parton densities increase with Q^2 at small x and decrease with large x. For low Q^2, the valence qurak flavors (uud, udd) contribute most to the nucleon structure. In contrast to this scenario, an increasing number of quark-antiquark pairs with a small momentum fraction x, known as sea quarks, are present at high Q^2. The entire quark number needs to hold the sum rule

provided below

$$\int_0^1 \{u(x)-\bar{u}(x)\}dx = 2; \int_0^1 \{d(x)-\bar{d}(x)\}dx = 1; \int_0^1 \{s(x)-\bar{s}(x)\}dx = 0, \quad (1.17)$$

which provides the proton quantum numbers. Furthermore, the total momentum of partons must follow the following momentum sum rule:

$$\sum_i \int_0^1 x q_i(x) dx = 1. \quad (1.18)$$

Perturbative QCD is unable to properly define PDFs as being non-perturbative entities. Instead, observables are fitted to experimental data to obtain these. However, the so-called QCD evolution equations allow one to investigate the rate at which PDFs change with the energy scales Q^2 and x within QCD. The QCD improved parton model predicts that the structure function is no more independent of Q^2 due to corrections coming from real gluon emission in $\alpha_s(Q^2)$. As a result, the F_2 structure function gets modified by QCD as

$$F_2(x, Q^2) = \sum_i e_i^2 x q_i(x, Q^2). \quad (1.19)$$

This results in a Q^2 dependence of both the structure function and parton distributions, which causes Bjorken's scaling violation. In order to find PDFs, one generally uses one of two methods: either build a reasonable but rough assumption or use neural network analysis to analyze the initial input distributions and evolve them to high Q^2 using QCD evolution equations. At the moment, numerous collaboration groups like MRST/MSTW [30–32], NNPDF [33, 34], HERAPDF [35, 36], CTEQ [37, 38], etc. are responsible for the parametrizations of PDFs for diverse kinematic domains. These parametrization groups have all incorporated the current high-precision data from the HERA and LHC into their analysis. The input data, parametrization

techniques, treatment of heavy quarks, coupling constant α_s value, and analytic approaches are where these groups diverge most. Since none of these groups can offer precise measurements for the entire kinematics domain, there is still no widely accepted set of PDFs.

1.6 QCD Evolution Equations

QCD introduces modifications to the parton model, leading to the resolution of scaling violations. It is possible to explicitly estimate the dependence of the structure function on Q^2 using QCD. But instead of revealing the exact value of F_2 for a given Q^2, it illustrates how F_2 varies with Q^2 from a given point. The perturbative determination of the Q^2 dependency of the PDFs is possible if Q^2 is large enough to maintain α_s small. In QCD, perturbation theory methods cannot be used directly to obtain the PDFs and structure functions. The primary theoretical tool for examining the energy scale dependency of parton distribution functions and, consequently, structure functions is the QCD evolution equations. The QCD evolution equations delineate the rate of variation of parton densities in relation to changes in the defining energy scale.

The Dokshitzer-Gribov-Lipatov-Altarelli-Parisi (DGLAP) [39–42] and Balitsky-Fadin-Kuraev-Lipatov (BFKL) [43–45] evolution equations are the two most well-known QCD evolution equations. The DGLAP equations can be used to compute the PDFs for any value of Q^2, provided the PDFs are at a certain initial scale Q_0^2, which will subsequently evolve to a particular Q^2. The DGLAP evolution adds up the contributions like $\alpha_s^n \ln(Q^2)^n$ in the perturbative expansion. At small-x contributions, however, which are carried by gluons, the logarithm of a small momentun fraction x increases the significance. The high-energy, or small-x, scattering case hence calls for a different strategy. $(\alpha_s \ln(1/x))^n$ is the sum of the leading logarithm (LL)

contributions in the BFKL evolution equation. The evolution equations mentioned are linear in parton density and are briefly summarized below.

DGLAP equation

Dokshitzer, Gribov, Lipatov, Altarelli, and Parisi proposed the DGLAP evolution equations in the late 1970s to characterize the evolution of PDFs with Q^2. DGLAP equations are sets of coupled equations that aggregate all leading Feynman diagrams, resulting in logarithmically amplified $\ln(Q^2)$ contributions to the cross section. The resummation of logarithms in transverse scale necessitates that the transverse momenta of subsequent steps in the emission diagrams be strongly ordered

$$Q^2 >> k_n^2 >> k_{n-1}^2 >> \cdots >> k_2^2 >> k_1^2. \tag{1.20}$$

For quark and gluon density, one can express the DGLAP equations in the following form:

$$\frac{\partial}{\partial \ln(Q^2)} \begin{pmatrix} q_i(x,Q^2) \\ g(x,Q^2) \end{pmatrix} = \frac{\alpha_s(Q^2)}{2\pi} \sum_{i=1}^{2N_f} \int_x^1 \frac{dy}{y} \begin{pmatrix} P_{qq}(x/y) & P_{qg}(x/y) \\ P_{gq}(x/y) & P_{gg}(x/y) \end{pmatrix} \begin{pmatrix} q_i(y,Q^2) \\ g(y,Q^2) \end{pmatrix}, \tag{1.21}$$

where $q_i(x,Q^2)$ represents quark density and $g(x,Q^2)$ for gluon density. The sum includes all quark and anti-quark flavors. Figure 1.4 depicts the graphic interpretations of the splitting functions P_{qq}, P_{qg}, P_{gq}, and P_{gg}. The splitting functions are defined as the probability of discovering a parton (quark or gluon) of type i with a momentum fraction x that is produced by a parton (quark or gluon) of type j with a larger momentum fraction $y > x$. The splitting functions P_{qg} and P_{gq} are independent of quark flavors due to charge conjugation and flavor independence of QCD's Lagrangian.

The splitting functions in perturbation theory can be expanded into the $\alpha_s(Q^2)$

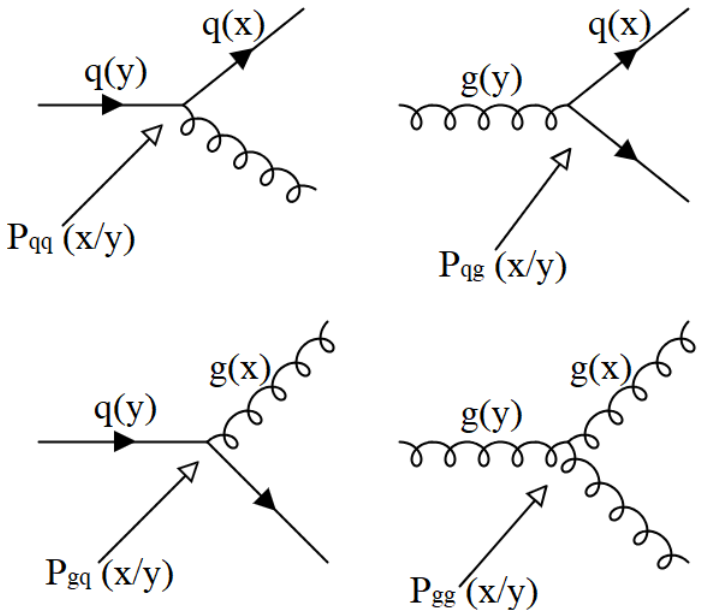

Figure 1.4: Splitting functions

power series as

$$P_{ab}(z,Q^2) = P_{ab}^{(0)}(z) + \Big(\frac{\alpha_s(Q^2)}{2\pi}\Big)P_{ab}^{(1)}(z) + \Big(\frac{\alpha_s(Q^2)}{2\pi}\Big)^2 P_{ab}^{(2)}(z) + \ldots, \quad (1.22)$$

with $z = x/y$. In the preceding expression, the terms $P^{(0)}$, $P^{(1)}$, and $P^{(2)}$ represent the leading order (LO), next-to-leading order (NLO), and next-to-next-to-leading order (NNLO) corrections to the splitting functions, respectively [46, 47]. The LO expressions are shown below [17]

$$P_{gq}^{(0)}(z) = \frac{4}{3}\Big[\frac{1+(1-z)^2}{z}\Big], \quad (1.23)$$

$$P_{qq}^{(0)}(z) = \frac{4}{3}\Big[\frac{1+z^2}{(1-z)_+} + \frac{3}{2}\delta(1-z)\Big], \quad (1.24)$$

$$P_{gg}^{(0)}(z) = 6\Big[\frac{1-z}{z} + \frac{z}{(1-z)_+} + z(1-z) + \frac{33-2n_f}{6}\delta(1-z)\Big]. \quad (1.25)$$

The "+" distribution is defined by the property

$$\int_0^1 dz \frac{f(z)}{(1-z)_+} = \int_0^1 dz \frac{f(z) - f(1)}{(1-z)}, \tag{1.26}$$

here, $(1-z)_+ = 1-z$ for $z < 1$, but for $z = 1$, it is infinite. The discrepancy at $z = 1$ complements soft gluon radiation and is compensated for by virtual gluon loop contributions.

For the singlet quark density, the DGLAP evolutions are given by

$$\frac{\partial}{\partial \ln(Q^2)} \sum(x, Q^2) = \frac{\alpha_s(Q^2)}{2\pi} (\sum \otimes P_{qq} + g \otimes 2n_f P_{qg}) \tag{1.27}$$

and

$$\frac{\partial}{\partial \ln(Q^2)} g(x, Q^2) = \frac{\alpha_s(Q^2)}{2\pi} (\sum \otimes P_{gq} + g \otimes P_{gg}), \tag{1.28}$$

with $\sum(x, Q^2) = \sum_i (q_i(x, Q^2) + \bar{q}_i(x, Q^2))$. The DGLAP technique can calculate the evolution of PDFs with respect to Q^2, but not at the beginning scale Q_0^2. As a result, at an initial scale, PDF information must be provided via non-perturbative methods or by parametrizing the x dependence at that scale. A typical parametrization function at a beginning scale (Q_0^2) is presented as

$$x f(x, Q_0^2) = A x^{\alpha} (1-x)^{\beta},$$

. The model parameters (A, α, and β) are determined by fitting experimental data.

The DGLAP equations neglect higher-order contributions such as $\alpha_s \ln(1/x)$. These leading $\ln(1/x)$ terms need to be resummed because, at finite order, the large logarithms in $1/x$ become significant in the perturbative expansion at small values of x, where the gluon cascade dominates the evolution. For high Q^2, the double leading logarithmic approximation (DLLA) is used, which resums the terms that comprise both the leading $\ln(1/x)$ and the leading $\ln(Q^2)$. Therefore, at small-x,

the major contribution to the gluon density growth may be identified by studying the DLLA of the DGLAP evolution, which is comparable to the contribution of the $(\alpha_s \ln(Q^2) \ln(1/x))^n$. The DLLA is valid when $\alpha_s \ln(Q^2) \ln(1/x) \sim 1$; however, both $\alpha_s \ln(Q^2)$ and $\alpha_s \ln(1/x)$ are small. However, at low Q^2, the DGLAP equation loses credibility as x decreases. In that case, an alternative equation, BFKL equation may be taken into account, which is discussed below.

BFKL equation

To describe the high-energy behavior of hadron processes, Balitsky, Fadin, Kuraev, and Lipatov first proposed the BFKL equation. The terms of the perturbation series enhanced by powers of $\ln(1/x)$ at small-x must be summed up. This equation uses gluon reggeization as the basis to sum up the leading logarithm contributions of the type $(\alpha_s \ln(1/x))^n$. The evolution equation for the unintegrated gluon distribution, $f(x, k_t)$, which depends on two independent variables—the transverse momentum k_t and the proton momentum fraction x carried by a gluon—generally corresponds to the BFKL approach. The distribution of the gluon density in $\ln(k_t)$ space is a key feature of this evolution. The evolution equation for BFKL in LO takes the generic form

$$-x\frac{\partial f(x,k_t^2)}{\partial x} = \frac{3\alpha_s(k_t^2)}{\pi} k_t^2 \int_{k_0'^2}^{\infty} \frac{dk_t'^2}{k_t'^2} \Big[\frac{f(x,k_t'^2) - f(x,k_t^2)}{|k_t'^2 - k_t^2|} + \frac{f(x,k_t^2)}{\sqrt{4k_t'^2 + k_t^2}} \Big], \quad (1.29)$$

where the infrared cut-off of the evolution is represented by $k_0'^2$ and the transverse momenta squared of the gluon in the initial and final states are denoted by $k_t'^2$ and k_t^2, respectively. The real emission of gluons is responsible for the first term in the square bracket, while the diagrams with virtual corrections correspond to the second term. The splitting of $k' \to k + q$ inside the hadron provides an interpretation for the real emission term found in the BFKL kernel. In contrast to the DGLAP equation,

the transverse momenta in BFKL have neither ordering nor constraints, whereas the longitudinal momenta are strongly ordered. Consequently, the BFKL kinematics can be written as follows if the momenta of the gluons in the ladder are labeled as $k_1, k_2, \ldots, k_n$

$$x_1 << x_2 << \cdots << x_n$$

$$k_{1t} \sim k_{2t} \sim \cdots \sim k_{nt}.$$

The BFKL evolution equation is more complicated than the DGLAP evolution equation because it includes contributions from operators with high twists. In its most basic form, the BFKL equation describes the amplitudes at non-zero momentum transfer in addition to the behavior of cross-sections at high-density QCD. Despite its success in characterizing QCD's high-energy asymptotics, the BFKL equation solution contains some discrepancies. The leading logarithmic BFKL equation breaks the unitarity limit at high collision energies, which is quite concerning. Another issue with the BFKL technique is that the transverse momenta of the gluons within the ladder drift to UV and IR [22]. The transverse momenta's drift towards IR results in a breach of the perturbative nature of the interaction assumption.

1.7 Gluon Saturation at Small-x and Nonlinear Evolution Equations

The crucial nature of gluons at small-x inside nucleons has been demonstrated by high-energy probes at colliders in recent years. In the limit of $x \to 0$, the gluon density inside nucleons rapidly increases, resulting in saturation effects. Understanding and measuring the gluon distribution at small-x in the lepton-nucleon or nucleon-nucleon DIS is crucial since it is the primary ingredient in various other analyses of different high-energy hadronic processes, and it may also probe novel effects arising from saturation effects [48–51]. As a result, there have been decades

of intense experimental activity and considerable phenomenological research at small-x, including different DIS at HERA and heavy ion collisions at RHIC. Furthermore, understanding this kinematic domain is crucial for computing various particle productions in proton-proton collisions at LHC.

In DIS investigations, the resolving power of a photon to detect a small-x parton rises; thus, the virtual photon may face multiple scattering off various partons for sufficiently small values of momentum fraction x. As a result, the gluon density increases sharply towards small-x. To comply with the Froissart-Martin bound on physical cross sections [52, 53], it is necessary to reduce the high gluon density, which exhibits fast growth at small-x. This bound, based on analyticity and unitarity constraints, sets restrictions on the upper limit for the cross section. The bound states that the total cross section must grow to comply with the rule $\sigma_{total} = \pi/m_{\pi}^2 \left(\ln s^2\right)$, where m_{π} represents the range of the strong force and s denotes nter of mass energy squared.

When $x \to 0$, the gluon density inside a proton increases rapidly for a fixed value of Q^2. The total transverse area within the proton occupied by gluons equals or exceeds the transverse area of the proton at some critical value $x = x_{crit}$. The probability that two gluons will interact is now indisputable due to the rapid growth of gluons at small-x. Recombination of gluons ($gg \to g$) thus becomes crucial in addition to the gluon emission process at small-x ($x < x_{crit}$). Saturation of the gluon density is the ultimate result of gluons recombining at small-x. The phenomenon of gluon saturation has arisen as one of the most intriguing problems, based on theoretical assumptions, but there is increasing evidence of its presence. Some experimental evidence of saturation effects include the early discovery of geometrical scaling phenomenon observed in HERA and the presence of geometrical scaling in jet productions in LHC data. It's worth noting that the size of the gluons affects the saturation, which in DIS is $r \sim 1/Q$. Larger-sized gluons will swarm

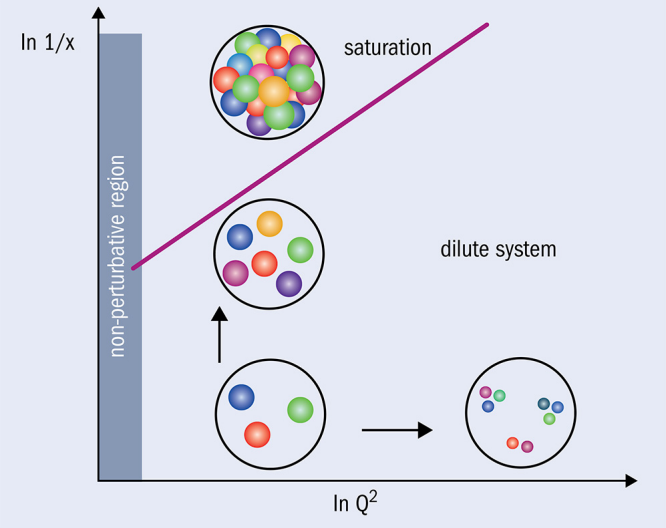

Figure 1.5: Schematic representation of the saturation of gluons inside the proton
Credit: Amanda Cooper Sarkar

the available transverse region inside the hadron earlier, causing them to re-interact, but small-sized gluons will delay saturation until higher energies are reached. A schematic representation of the gluon saturation process is shown in Figure 1.5. The saturated regime and the dilute regime are separated by a saturation scale, Q_s, which is a conventional transverse momentum scale.

DGLAP and BFKL being linear evolution equations unable to address the non-linear phenomena of gluon recombination and saturation at small-x and hence fail to account for underlying physics in high-density QCD. It is vital to understand the underlying physics in saturation regions of gluons at small-x. The nonlinear QCD evolution equations come into play in saturation region, which helps in understanding the physics in that region. Therefore, to describe the gluon recombination and saturation effect, the linear evolution equations have to be replaced by the nonlinear QCD evolution equations. The nonlinear evolution equations have important features dealing with the saturation effect. They contain damping terms that reflect the saturation effect arising out of gluon-gluon recombination. Thus, studying nonlinear QCD evolution equations and their solutions is crucial for phenomenological studies

at existing and future experimental facilities.

Several nonlinear QCD evolution equations have been proposed based on the two linear evolution equations, DGLAP and BFKL, in order to address nonlinear physics in high-density QCD. Gribov, Levin, and Ryskin (GLR) [48] and Muller and Qiu (MQ) [51] performed the first perturbative QCD calculations that included gluon recombination. They proposed a new nonlinear evolution equation using an extra nonlinear quadratic in the gluon density. This new nonlinear evolution equation, also known as the GLR-MQ equation, is an updated version of the DGLAP equation that includes certain gluon recombination corrections. There are various nonlinear evolution equations that use nonlinear corrections to the DGLAP and BFKL evolutions. For instance, Modified DGLAP (MD-DGLAP) [54, 55] is a DGLAP-based nonlinear equation, while Balitsky-Kovchegov (BK) [56–59], Modified-BFKL (MD-BFKL) [60] equation, and Jalilian-Marian-Iancu-McLerran-Weigert-Leonidov-Kovner (JIMWLK) equation [61–64] are BFKL-based nonlinear evolution equations. The BK equation serves as the most suitable evolution equation at small-x where nonlinear saturation effects play an important rule. This equation is a mean-field approximation of the more complex JIMWLK equation.. Despite numerous numerical studies, an exact analytical solution to this equation remains elusive due to its complex nature. Thus, analytical studies of the BK equation are required to understand the nonlinear physics at small-x. In this thesis, we are going to study the BK nonlinear equation and its applications to various phenomena inside hadrons at small-x.

1.8 High Energy Experiments and PDF Groups

High Energy Experiments

To determine the observables, like structure functions, a high-energy probe needs a precise experimental setup, which has been achieved over the past few decades by various high energy experiments. In recent years, these have contributed to the exploration of particle physics at both high energy and high precision frontiers. The electron-proton DIS experiment, carried out at SLAC in 1968 in California, USA, was the first high energy experiment in this row [65]. Subsequently, several additional experiments have been established to examine the structure of hadrons, including E26 [66], Bologna-CERN-Dubna-Munich-Saclay (BCDMS) [67], New Muon Collaboration (NMC) [68], European Muon Collaboration (EMC) [69], and HERA at DESY [26, 29, 70]. The principal initiative at CERN, the Large Hadron Collider (LHC) [71, 72], is now executing the latest high-energy experiments. The LHC is now the largest and most powerful experimental laboratory constructed by humans. Numerous further prospective high-energy initiatives, such as the Large Hadron Electron Collider (LHeC) at CERN and the Electron-Ion Collider (EIC) at Brookhaven National Laboratory (BNL), are now in progress. Concise summaries of these experiments are presented here.

SLAC

The Stanford Linear Accelerator Center (SLAC) hosts the Stanford Linear Accelerator, a 3.2-kilometer (2-mile) linear accelerator built in 1966. It is now operated by Standford University and sponsored by the Department of Energy, USA. In 1968, SLAC carried out the first DIS experiments to investigate proton structure, exploring the kinematic range of $0.06 \leq x \leq 0.9$ and $0.6 \leq Q^2 \leq 50$ GeV^2. The notable

discoveries at SLAC that produced three nobel prizes in physics were: in 1976, for the discovery of the first charm particle, the J/ψ meson; in 1990, for the discovery of the existence of quarks inside nucleons; and in 1995, for the discovery of the tao lepton.

BCDMS

The BCDMS experiment at CERN performed a DIS experiment with muons on hydrogen targets at beam strengths of 100,120, $200, and$280 GeV. This experiment spanned the kinematic range of $0.06 \leq x \leq 0.8$ to $7 \leq Q^2 \leq 260$ GeV^2. The structure functions were calculated using the ratio R_{QCD}, which indicates the ratio of longitudinally polarized virtual photon absorption cross-section to transversely polarized. The total normalization error was roughly 3%.

EMC

The EMC experiment at CERN used a muon beam with a beam energy of 280 GeV on a target made of a heavier element, like deuterium. The kinematic range of the experiment was $0.0025 \leq x \leq 0.14$ and $0.25 \leq Q^2 \leq 7.2$ GeV^2, which offered a good description of the measurements. However, the rest of their measurements are overtaken by the more precise measurements of the NMC experiment, given below. The entire normalization error was 7%.

NMC

As an extension of the EMC experiment, the new muon collaoration used upgraded equipment to perform the NMC experiment in the $M2$ muon beam line of the CERN SPS. In this experiment, The differential cross sections for protons and deuteron were determined concurrently employing two identical pairs of $3m$-long targets in the NMC experiment exposed off and on to the muon beam. The relative normalization

between the proton and deuteron structure functions was considerably less ambiguous as a result of these measurements. It is reported that the overall normalization error is 2%. To find structure functions, an iterative approach based on the experiment's Monte Carlo simulation was used. Individual simulations were run for every data collection session to account for variations in the beam and the detector. The structure function, $F_2(x, Q^2)$ were determined by comparing the accepted Monte Carlo events and the normalized data outputs. Proton and deuteron structure functions, F_2^p and F_2^d, were measured by inclusive DIS using beams of 90, 120, 200, and 280 GeV muons on hydrogen and deuterium targets in the kinematic range $0.006 \leq x \leq 0.6$ and $0.5 \leq Q^2 \leq 75$ GeV^2. The structure functions were computed using a fixed parametrization of the ratio, $R(x, Q^2)$, which was obtained from a global analysis of SLAC data and an initial selection of F_2.

E665

In the fixed-target muon scattering experiment E665 at Fermilab, muon beams with the highest energy of around 490 GeV are used. In addition to measuring structure functions and ratios, the E665 experiment also examined the hadronic final states produced via muon interactions and collected data from liquid hydrogen and deuterium targets as well as heavy targets. The kinematic range of the F_2 measurements is as follows: $8.9 \times 10^{-4} \leq x \leq 0.39$ and $0.2 \leq Q^2 \leq 75$ GeV^2. The reported normalization error is 1.8%. The E665 and NMC measurements have a considerable overlap in x and Q^2, and the two measurements agree well within the overlap region. At the lower Q^2 region with fixed x, the E665 data agree well with the HERA data as well.

H1 and ZEUS

HERA (Hadron-Electron Ring Accelerator), an electron-proton collider at DESY in Hamburg, Germany, is used to explore DIS processes using two main experiments, H1 and ZEUS. A truly worldwide scientific collaboration, the ZEUS collaboration is led by 450 physicists from 12 countries, whereas H1 is an international collaboration of about 250 scientists from 20 institutes and 12 countries. The HERA collider's initial operation provides an essential benchmark for proton structure measurements. The collaborations at HERA measured both the NC and CC cross sections in inclusive $e^{\pm}p$ DIS, colliding proton beam energy of 920 GeV with electron beam energy of 27.5 GeV. This produced an enormous center of mass energy of $\sqrt{s} \approx 320$ GeV. In the H1 and ZEUS experiments, the highest value of Q^2 was 90, 200 GeV^2; however, the calibrated x-range has been substantially expanded to a smaller value of $x \sim 10^{-5}$. HERA had two stages of operation. HERA-I functioned from 1992 to 2000, while HERA-II operated from 2002 to 2007. The H1 and ZEUS collaborations use HERA-I data to achieve the most exact determination of proton structure. HERA-I primarily utilized positrons to operate because of constraints on the lifetime of electron beams. For HERA-II, this problem has been resolved, and because HERA used electron beams for operation from 2004 to 2006, the xF_3 structure function may be measured with increased precision. The direct measurement of F_L were obtained from a series of operations carried out by HERA in 2007 with proton beam intensities of 460 and 575 GeV. An accurate fit of PDFs the proton was provided by the H1-ZEUS combined data, which have significantly reduced uncertainties than the individual experiments. In both investigations, R_{QCD} has been used to obtain the F_2 structure function. The NC data has a kinematic range of $6 \times 10^{-7} \leq x \leq 0.65$ and $0.045 \leq Q^2 \leq 3000$ GeV^2 for inelasticity values y ranging from 0.005 to 0.95. The CC data has a kinematic range of $1.3 \times 10^{-2} \leq x \leq 0.40$ and $300 \leq Q^2 \leq 3000$ GeV^2 for

y values ranging from 0.037 to 0.76. Despite the fact that HERA's functioning terminated in 2007, analyses of its data files are still being conducted by H1 and ZEUS collaboration, with exceptional results.

LHC

The Large Hadron Collider (LHC), the largest and most potent particle accelerator globally, was constructed by CERN in partnership with numerous universities and laboratories. More than 10,000 scientists and engineers from over 100 countries. The LHC, weighing over 38,000 tons, is situated in Geneva, Switzerland, and extends 27 kilometers within a circular tunnel that lies 100 meters beneath the Swiss-French border. An electrical issue led to the cessation of operations at the LHC in 2008, coinciding with the initial successful circulation of proton beams in the main ring. In 2009, the LHC successfully cycled the proton beams, recording the initial proton-proton collisions, each with an energy of 450 GeV. An injection energy of 450 GeV per beam was reported. In 2010, two proton beams, each with an energy of 3.5 TeV, were collided, representing the highest-energy particle collision recorded at that time. In 2012, the LHC's beam energy increased to 4 TeV per proton and subsequently to 6.5 TeV in 2015. Seven investigations are underway at the LHC to investigate the many particles generated by the accelerator. The Toroidal LHC Apparatus (ATLAS) and the Compact Muon Solenoid (CMS), the largest of these experiments, employ two separately constructed general-purpose detectors to investigate phenomena from dark matter and additional dimensions to the search for the Higgs boson. The A Large Ion Collider Experiment (ALICE) is a heavy-ion detector intended to study the creation of quark-gluon plasma, a high-density quantum chromodynamics phenomenon. The LHCb experiment seeks to examine the differences between matter and antimatter. Protons, heavy ions, and forward particles are examined by the Total Elastic and Diffractive Cross Section Measurement (TOTEM) and LHC

forward (LHCf) studies. Established in 2010, the Monopole and Exotics Detector at the LHC (MOEDAL) investigates magnetic monopoles. The Higgs boson, predicted almost 50 years earlier, was confirmed as the particle with a mass of approximately 126 GeV in 2012 by the ATLAS and CMS experiments at the LHC. The identification of the Higgs boson at the LHC is a pivotal achievement in physics, leading to F. Englert and P. W. Higgs receiving the Nobel Prize in Physics in 2013 for their theoretical prediction of the Higgs process.

EIC

The Electron-Ion Collider (EIC) is a projected particle accelerator collider developed by BNL and approved by the US Department of Energy. The EIC is intended to collide spin-polarized beams of electrons and ions in order to explore the characteristics of nuclear matter in depth using deep inelastic scattering. Scientists from BNL and Jefferson Lab will work with researchers from all over the world to develop the EIC. The EIC user group includes approximately 1400 physicists from 290 laboratories and universities in 38 countries. The EIC will be the world's first world-class particle collider, measuring 2.4 miles in circumference. It will direct beams of high-energy polarized electrons into collisions with polarized protons and atomic nuclei, yielding precise 3D illustrations of their internal structures. Experiments at the EIC will help scientists understand the secrets of nature's strongest force and investigate how tiny particles known as quarks and gluons contribute to the mass, spin, and other aspects of all observable matter. EIC will examine the physics of high-density QCD at small-x and explore phenomena such as gluon recombination and saturation, as well as their evidence of existence. In addition, the EIC study will shed light on how it changed from a split second after the Big Bang, or around 14 billion years ago, until the present. For many years to come, this investigation into an exciting area of physics will advance science and technology.

PDF Groups

One of the fundamental components needed to calculate any observable involving hadrons is the PDFs. The evolution of PDFs, expressed in the form of PDF evolution equations, is a critical test of our comprehension of QCD dynamics. Accurate understanding of these PDFs is a necessary precondition to recognize any potential signature from physics that goes beyond the Standard Model. In contrast, a precise assessment of the errors related to the PDFs is essential for producing reliable phenomenological predictions at hadronic colliders like the LHC. Recently, a significant amount of theoretical and experimental efforts have been focused on precisely determining the nucleon's parton distributions. Global fits to data from a variety of fixed target experiments, including the LHC at CERN, the HERA at DESY, and the TEVATRON at Fermilab, have been used to actively determine and update PDFs. The majority of the data that has been utilized in the past comes from the jet production, Drell-Yan (DY), and DIS processes. The development of modern colliders like the LHC has resulted in an enormous data flow, which has greatly aided phenomenological applications. The global PDF groups that are now in operation include HERAPDF, ABM, CTEQ/CT, JR, MSTW/MMHT, and NNPDF. Since numerous groups have different PDFs with different parametrization methods for the data, a common library, LHAPDF [74], was created to keep a large amount of PDFs that are readily available. Additionally, a web-based program called APFEL Web was created recently [75, 76]. It is based on updated versions of LHAPDF and offers a graphical representation of PDFs, making it possible to compute PDFs along with the errors that come along with them. We may also compare PDFs from different global PDF groups with this tool. The PDF parametrization gropus NNPDF and CTEQ collaboration, whose data sets are used in this thesis, is briefly described below.

NNPDF

The Neural Network PDFs (NNPDF) collaboration uses modern artificial intelligence techniques to determine the proton's structure. An essential component of the physics program of CERN's Large Hadron Collider is a precise comprehension of the so-called PDFs of the proton, which characterize its structure in terms of its quark and gluon constituents. It has played a crucial role in the Higgs boson's discovery. One of the biggest challenges to the search for new physics is its insufficient knowledge. PDFs must be carefully retrieved from the data by comparing theoretical predictions and experimental findings; they cannot be computed from basic principles. NNPDF employs neural networks developed with genetic algorithms to determine PDFs accurately. These networks are then used to build a Monte Carlo representation of PDFs and associated uncertainties, which is a probability distribution in a space of functions. Recently, NNPDF released a new set of PDFs based on a fully global dataset and machine learning techniques that display paths to the proton structure with 1% accuracy [77].

CTEQ

The Coordinated Theoretical-Experimental Project on QCD (CTEQ) is a multi-institutional collaboration focused on high-energy physics, including QCD and its implications for the Standard Model and beyond. CTEQ studies parton distribution functions. CTEQ-TEA (CTEQ Tung Et Al.) [78] provides general-purpose parton distributions in the nucleon up to the next-to-next-to-leading order (NNLO); tools for fast PDF analysis, PDF updating, and PDF set combination; and specialized PDFs for massive quark computations. The CJ (CTEQ-Jefferson Lab) Collaboration uses global QCD fits of parton distribution functions (PDFs) to study the quark and gluon structure of the nucleon. With special attention to the large-x region,

these parametrize a wide range of data, such as proton-proton collisions (lepton pair generation, W-boson, and jet production), deep-inelastic lepton-nucleon scattering, and other reactions. CJ Collaboration presented the results of a novel global next-to-leading order fit of parton distribution functions in Ref. [79]. This fit reduces cuts on W and Q, allowing for more data at high values of x. The nCTEQ (nuclear CTEQ) project is an extension of the CTEQ collaborative effort to identify nuclear parton distribution functions (nPDFs). It extends the free-proton PDF framework to the nuclear situation by determining the densities of protons bound inside a nucleus. In Ref. [80], nCTEQ introduces the nCTEQ15 set of nuclear parton distribution functions (nPDFs) with uncertainties.

1.9 Outline of the Thesis

In this thesis, we conducted a phenomenological study of the nonlinear QCD evolution equation at high density QCD in the context of nonlinear phenomena within hadrons at small-x. We focused on the BK nonlinear evolution equation and its properties, as they are the most relevant QCD evolution equations for small-x physics. The BK equation has been widely studied numerically, but substantial analytical studies have yet to be completed. Thus, in this thesis, we looked into the BK equation and attempted to solve it analytically. Then we will look into its analytical solution in the gluon saturation region, where nonlinear effects are likely to play an essential role, and apply it to a variety of phenomenological aspects at small-x. The thesis is structured into chapters as follows:

In chapter 2, we examine the BK evolution equation, a pivotal nonlinear parton evolution equation for small-x. We provided an approximate analytical solution to the BK problem via the homotopy perturbation method (HPM). We obtained the gluon saturation momentum from the resultant solution and contrasted it with the

numerical analysis of the BK equation.

In chapter 3, we examine the proton structure function $F_2^p(x, Q^2)$ at small-x employing the BK evolution equation. In the color dipole framework of deep inelastic scattering (DIS), the structural function $F_2^p(x, Q^2)$ is derived using the dipole-proton scattering amplitude $N(k, Y)$, which is obtained via the solution of the BK equation. Additionally, we have derived the integrated gluon density $xg(x, Q^2)$ utilizing the BK solution and contrasted it with the global PDF fitting groups, NNPDF3.1sx and CT18. This chapter delineates the behavior of $F_2^p(x, Q^2)$ within the kinematic range of $10^{-5} \leq x \leq 10^{-2}$ and $2.5 \leq Q^2 \leq 60$ GeV^2. The results for $F_2^p(x, Q^2)$ are compared with those from the H1 Collaboration at HERA and the PDF parametrization group NNPDF3.1sx.

In chapter 4, we examine the theoretical prediction of exclusive vector meson generation within the color dipole framework of electron-proton deep inelastic scattering. We have computed both the differential and total cross-sections for the formation of J/Ψ and ρ^0 in accordance with the BK evolution equation. Furthermore, we have illustrated the ratio of the longitudinal to the transverse cross-section for the formation of J/Ψ and ρ^0 vector mesons as a function of Q^2. Our analysis incorporates two prominent vector meson wave function models, Boosted Gaussian and Gaus-LC, which exhibit minor sensitivity to the selected vector meson wave functions. This chapter compares theoretical predictions with current experimental data for exclusive vector meson generation.

In chapter 5, we encapsulate and delineate our conclusions alongside potential future prospects.

Bibliography

[1] Philip Ball. *The elements: a very short introduction*. OUP Oxford, 2004.

[2] M Gell-Mann. A schematic model of baryons and mesons. *Physics Letters*, 8(3):214–215, 1964.

[3] George Zweig. An su _3 model for strong interaction symmetry and its breaking. Technical report, CM-P00042884, 1964.

[4] RP Feynman. Photon–hadron interactions. *Reading*, 1972.

[5] Robert Oerter. *The theory of almost everything: The standard model, the unsung triumph of modern physics*. Penguin, 2006.

[6] Sheldon L Glashow. Partial-symmetries of weak interactions. *Nuclear physics*, 22(4):579–588, 1961.

[7] Steven Weinberg. A model of leptons. *Physical review letters*, 19(21):1264, 1967.

[8] A SALAM. Weak and electromagnetic interactions. In *Elementary Particle Theory, Proceedings of the Nobel Symposium Held 1968 at Lerum, Sweden*, pages 367–377, 1968.

[9] G Arnison, A Astbury, B Aubert, C Bacci, G Bauer, A Bézaguet, R Böck, TJV Bowcock, M Calvetti, T Carroll, et al. Experimental observation of isolated large transverse energy electrons with associated missing energy at s= 540 gev. *Physics Letters B*, 122(1):103–116, 1983.

[10] Fumio Abe, H Akimoto, A Akopian, MG Albrow, SR Amendolia, D Amidei, J Antos, C Anway-Wiese, S Aota, G Apollinari, et al. Observation of top quark

production in p p collisions with the collider detector at fermilab. *Physical review letters*, 74(14):2626, 1995.

[11] K Kodama, N Ushida, C Andreopoulos, N Saoulidou, G Tzanakos, P Yager, B Baller, D Boehnlein, Walter Freeman, B Lundberg, et al. Observation of tau neutrino interactions. *Physics Letters B*, 504(3):218–224, 2001.

[12] Adrian Cho. Higgs boson makes its debut after decades-long search. *Science*, 337(6091):141–143, 2012.

[13] Harald Fritzsch, Murray Gell-Mann, and Heinrich Leutwyler. Advantages of the color octet gluon picture. *Physics Letters B*, 47(4):365–368, 1973.

[14] Francis Halzen and Alan D Martin. *Quark & Leptons: An introductory course in modern particle physics*. John Wiley & Sons, 2008.

[15] David J Gross and Frank Wilczek. Asymptotically free gauge theories. i. *Physical Review D*, 8(10):3633, 1973.

[16] David J Gross and Frank Wilczek. Asymptotically free gauge theories. ii. *Physical Review D*, 9(4):980, 1974.

[17] H David Politzer. Asymptotic freedom: An approach to strong interactions. *Physics Reports*, 14(4):129–180, 1974.

[18] Alexandre Deur, Stanley J Brodsky, and Guy F de Teramond. The qcd running coupling. *Progress in Particle and Nuclear Physics*, 90:1–74, 2016.

[19] Richard P Feynman. Very high-energy collisions of hadrons. *Physical Review Letters*, 23(24):1415, 1969.

[20] James D Bjorken and Emmanuel A Paschos. Inelastic electron-proton and γ-proton scattering and the structure of the nucleon. *Physical Review*, 185(5):1975, 1969.

[21] JL Abelleira Fernandez, C Adolphsen, Ahmet Nuri Akay, H Aksakal, JL Albacete, S Alekhin, P Allport, V Andreev, RB Appleby, E Arikan, et al. A large hadron electron collider at cern report on the physics and design concepts for machine and detector. *Journal of Physics G: Nuclear and Particle Physics*, 39(7):075001, 2012.

[22] Yuri V Kovchegov and Eugene Levin. *Quantum chromodynamics at high energy*. Cambridge University Press, 2013.

[23] James D Bjorken. Asymptotic sum rules at infinite momentum. *Physical Review*, 179(5):1547, 1969.

[24] LF Abbott, WB Atwood, and R Michael Barnett. Quantum-chromodynamic analysis of en deep-inelastic scattering data. *Physical Review D*, 22(3):582, 1980.

[25] Stephen L Adler and Wu-Ki Tung. Breakdown of asymptotic sum rules in perturbation theory. *Physical Review Letters*, 22(18):978, 1969.

[26] Catherine Adloff, V Andreev, B Andrieu, T Anthonis, V Arkadov, A Astvatsatourov, A Babaev, J Bähr, P Baranov, E Barrelet, et al. On the rise of the proton structure function f_2 towards low x. *Physics Letters B*, 520(3-4):183–190, 2001.

[27] H1 Collaboration. Measurement and qcd analysis of neutral and charged current cross sections at hera. *The European Physical Journal C-Particles and Fields*, 30(1):1–32, 2003.

[28] J Breitweg, M Derrick, D Krakauer, S Magill, D Mikunas, B Musgrave, J Repond, R Stanek, RL Talaga, R Yoshida, et al. Measurement of the proton structure function f_2 and $\sigma_{tot}^{\gamma p}$ at low q^2 and very low x at hera. *Physics Letters B*, 407(3-4):432–448, 1997.

[29] S Chekanov, M Derrick, D Krakauer, JH Loizides, S Magill, S Miglioranzi, B Musgrave, J Repond, R Yoshida, Margarita CK Mattingly, et al. High-q^2 neutral current cross sections in e^+ p deep inelastic scattering at $\sqrt{s} = 318$ gev. *Physical Review D—Particles, Fields, Gravitation, and Cosmology*, 70(5):052001, 2004.

[30] AD Martin, RG Roberts, W James Stirling, and RS Thorne. Nnlo global parton analysis. *Physics Letters B*, 531(3-4):216–224, 2002.

[31] AD Martin, RG Roberts, WJ Stirling, and RS Thorne. Physical gluons and high-et jets. *Physics Letters B*, 604(1-2):61–68, 2004.

[32] Alan D Martin, W James Stirling, Robert S Thorne, and Graeme Watt. Parton distributions for the lhc. *The European Physical Journal C*, 63(2):189–285, 2009.

[33] Richard D Ball, Valerio Bertone, Stefano Carrazza, Luigi Del Debbio, Stefano Forte, Patrick Groth-Merrild, Alberto Guffanti, Nathan P Hartland, Zahari Kassabov, José I Latorre, et al. Parton distributions from high-precision collider data: Nnpdf collaboration. *The European Physical Journal C*, 77:1–75, 2017.

[34] Rabah Abdul Khalek, Richard D Ball, Stefano Carrazza, Stefano Forte, Tommaso Giani, Zahari Kassabov, Rosalyn L Pearson, Emanuele R Nocera, Juan Rojo, Luca Rottoli, et al. Parton distributions with theory uncertainties: general formalism and first phenomenological studies: Nnpdf collaboration. *The European Physical Journal C*, 79:1–61, 2019.

[35] AM Cooper-Sarkar. Pdf fits at hera. *arXiv preprint arXiv:1112.2107*, 2011.

[36] Zhiqing Zhang. Hera inclusive neutral and charged current cross sections and a new pdf fit, herapdf 2.0. *arXiv preprint arXiv:1511.05402*, 2015.

[37] Pavel M Nadolsky, Hung-Liang Lai, Qing-Hong Cao, Joey Huston, Jon Pumplin, Daniel Stump, Wu-Ki Tung, and C-P Yuan. Implications of cteq global analysis for collider observables. *Physical Review D—Particles, Fields, Gravitation, and Cosmology*, 78(1):013004, 2008.

[38] Tie-Jiun Hou, Sayipjamal Dulat, Jun Gao, Marco Guzzi, Joey Huston, Pavel Nadolsky, Jon Pumplin, Carl Schmidt, Daniel Stump, and C-P Yuan. Cteq-tea parton distribution functions and hera run i and ii combined data. *Physical Review D*, 95(3):034003, 2017.

[39] Vladimir Naumovich Gribov and LN Lipatov. Deep inelastic ep scattering in perturbation theory. *Sov. J. Nucl. Phys.*, 15:438–450, 1972.

[40] V Gribov and L Lipatov. e+ e-pair annihilation and deep inelastic ep scattering in perturbation theory. *Soviet Journal of Nuclear Physics*, 15:675–675, 1972.

[41] Yu L Dokshitser. Calculation of structure functions of deep-inelastic scattering and e+ e-annihilation by perturbation theory in quantum chromodynamics. *Soviet Journal of Experimental and Theoretical Physics*, 46:641, 1977.

[42] Guido Altarelli and Giorgio Parisi. Asymptotic freedom in parton language. *Nuclear Physics B*, 126(2):298–318, 1977.

[43] Eh A Kuraev, LN Lipatov, and Victor S Fadin. Multireggeon processes in the yang-mills theory. *Zhurnal Ehksperimental'noj i Teoreticheskoj Fiziki*, 71(9):840–855, 1976.

[44] EA Kuraev, LN Lipatov, and VS Fadin. The pomeranchuk singularity in nonabelian gauge theories. *Sov. Phys. JETP*, 45:199, 1977.

[45] Yu Yu Balitsky and LN Lipatov. The pomeranchuk singularity in quantum chromodynamics. *Yad. Fiz.*, 28:1597–1611, 1978.

[46] Andreas Vogt, S Moch, and JAM1109 Vermaseren. The three-loop splitting functions in qcd: the singlet case. *Nuclear Physics B*, 691(1-2):129–181, 2004.

[47] G Curci, W Furmanski, and Roberto Petronzio. Evolution of parton densities beyond leading order: the non-singlet case. *Nuclear Physics B*, 175(1):27–92, 1980.

[48] Leonid Vladimirovič Gribov, Eugene M Levin, and Michail G Ryskin. Semi-hard processes in qcd. *Physics Reports*, 100(1-2):1–150, 1983.

[49] Wei Zhu, Jianhong Ruan, Jifeng Yang, and Zhenqi Shen. Contributions of gluon recombination to saturation phenomena. *Physical Review D*, 68(9):094015, 2003.

[50] J Kwiecinski. Theoretical issues of small x physics. *Journal of Physics G: Nuclear and Particle Physics*, 22(6):685, 1996.

[51] Alfred H Mueller and Jianwei Qiu. Gluon recombination and shadowing at small values of x. *Nuclear Physics B*, 268(2):427–452, 1986.

[52] Marcel Froissart. Asymptotic behavior and subtractions in the mandelstam representation. *Physical Review*, 123(3):1053, 1961.

[53] A Martin. Unitarity and high-energy behavior of scattering amplitudes. *Physical Review*, 129(3):1432, 1963.

[54] Wei Zhu. A new approach to parton recombination in the qcd evolution equations. *Nuclear Physics B*, 551(1-2):245–274, 1999.

[55] Wei Zhu and Jianhong Ruan. A new modified altarelli-parisi evolution equation with parton recombination in proton. *Nuclear Physics B*, 559(1-2):378–392, 1999.

[56] Ian Balitsky. Operator expansion for diffractive high-energy scattering. *arXiv preprint hep-ph/9706411*, 1997.

[57] Yuri V Kovchegov. Small-x f 2 structure function of a nucleus including multiple pomeron exchanges. *Physical Review D*, 60(3):034008, 1999.

[58] Yuri V Kovchegov. Unitarization of the bfkl pomeron on a nucleus. *Physical Review D*, 61(7):074018, 2000.

[59] Ian Balitsky. Effective field theory for the small-x evolution. *Physics Letters B*, 518(3-4):235–242, 2001.

[60] Jianhong Ruan, Zhenqi Shen, Jifeng Yang, and Wei Zhu. Antishadowing effects in the unitarized bfkl equation. *Nuclear Physics B*, 760(1-2):128–144, 2007.

[61] Ian Balitsky. Operator expansion for high-energy scattering. *Nuclear Physics B*, 463(1):99–157, 1996.

[62] Jamal Jalilian-Marian, Alex Kovner, Andrei Leonidov, and Heribert Weigert. The bfkl equation from the wilson renormalization group. *Nuclear Physics B*, 504(1-2):415–431, 1997.

[63] Edmond Iancu, Andrei Leonidov, and Larry McLerran. Nonlinear gluon evolution in the color glass condensate: I. *Nuclear Physics A*, 692(3-4):583–645, 2001.

[64] Heribert Weigert. Unitarity at small bjorken x. *Nuclear Physics A*, 703(3-4):823–860, 2002.

[65] LW Whitlow, EM Riordan, S Dasu, Stephen Rock, and A Bodek. Precise measurements of the proton and deuteron structure functions from a global analysis of the slac deep inelastic electron scattering cross sections. *Physics Letters B*, 282(3-4):475–482, 1992.

[66] C Chang, KW Chen, DJ Fox, A Kotlewski, Paul F Kunz, LN Hand, S Herb, A Russell, Y Watanabe, SC Loken, et al. Observed deviations from scale invariance in high-energy muon scattering. *Physical Review Letters*, 35(14):901, 1975.

[67] Alberto C Benvenuti, D Bollini, G Bruni, FL Navarria, A Argento, W Lohmann, L Piemontese, J Strachota, P Zavada, S Baranov, et al. A high statistics measurement of the deuteron structure functions f2 (x, q2) and r from deep inelastic muon scattering at high q2. *Physics Letters B*, 237(3-4):592–598, 1990.

[68] Michele Arneodo, A Arvidson, B Badełek, M Ballintijn, Guenter Baum, J Beaufays, IG Bird, P Björkholm, M Botje, C Broggini, et al. Measurement of the proton and the deuteron structure functions, f2p and f2d. *Physics Letters B*, 364(2):107–115, 1995.

[69] M Arneodo, A Arvidson, JJ Aubert, B Badelek, J Beaufays, CP Bee, C Benchouk, G Berghoff, IG Bird, D Blum, et al. Measurements of the nucleon structure function in the range 0.002< x< 0.17 and 00.2< q2< 8 gev2 in deuterium, carbon and calcium. *Nuclear Physics B*, 333(1):1–47, 1990.

[70] Francise D Aaron, H Abramowicz, I Abt, L Adamczyk, M Adamus, Al-daya Martin, C Alexa, V Andreev, S Antonelli, P Antonioli, et al. Combined measurement and qcd analysis of the inclusive e±p scattering cross sections at hera. *Journal of High Energy Physics*, 2010(1):1–63, 2010.

[71] Georges Aad, Tatevik Abajyan, Brad Abbott, Jalal Abdallah, S Abdel Khalek, Ahmed Ali Abdelalim, R Aben, B Abi, M Abolins, OS AbouZeid, et al. Observation of a new particle in the search for the standard model higgs boson with the atlas detector at the lhc. *Physics Letters B*, 716(1):1–29, 2012.

[72] Serguei Chatrchyan, Vardan Khachatryan, Albert M Sirunyan, Armen Tumasyan, Wolfgang Adam, Ernest Aguilo, Thomas Bergauer, Marko Dragicevic, Janos Erö, Christian Fabjan, et al. Observation of a new boson at a mass of 125 gev with the cms experiment at the lhc. *Physics Letters B*, 716(1):30–61, 2012.

[73] A Accardi, JL Albacete, M Anselmino, N Armesto, EC Aschenauer, Alessandro Bacchetta, D Boer, WK Brooks, T Burton, N B Chang, et al. Electron-ion collider: The next qcd frontier: Understanding the glue that binds us all. *The European Physical Journal A*, 52:1–100, 2016.

[74] Andy Buckley, James Ferrando, Stephen Lloyd, Karl Nordström, Ben Page, Martin Rüfenacht, Marek Schönherr, and Graeme Watt. Lhapdf6: parton density access in the lhc precision era. *The European Physical Journal C*, 75:1–20, 2015.

[75] Valerio Bertone, Stefano Carrazza, and Juan Rojo. Apfel: a pdf evolution library with qed corrections. *Computer Physics Communications*, 185(6):1647–1668, 2014.

[76] Stefano Carrazza, Alfio Ferrara, Daniele Palazzo, and Juan Rojo. Apfel web: a web-based application for the graphical visualization of parton distribution functions. *Journal of Physics G: Nuclear and Particle Physics*, 42(5):057001, 2015.

[77] Richard D Ball, Stefano Carrazza, Juan Cruz-Martinez, Luigi Del Debbio, Stefano Forte, Tommaso Giani, Shayan Iranipour, Zahari Kassabov, Jose I Latorre, Emanuele R Nocera, et al. The path to proton structure at 1% accuracy: Nnpdf collaboration. *The European Physical Journal C*, 82(5):428, 2022.

[78] Sayipjamal Dulat, Tie-Jiun Hou, Jun Gao, Marco Guzzi, Joey Huston, Pavel Nadolsky, Jon Pumplin, Carl Schmidt, Daniel Stump, and C-P Yuan. New par-

ton distribution functions from a global analysis of quantum chromodynamics. *Physical Review D*, 93(3):033006, 2016.

[79] A Accardi, ME Christy, CE Keppel, W Melnitchouk, P Monaghan, JG Morfin, and JF Owens. New parton distributions from large-x and low-q 2 data. *Physical Review D—Particles, Fields, Gravitation, and Cosmology*, 81(3):034016, 2010.

[80] K Kovařík, A Kusina, T Ježo, DB Clark, C Keppel, F Lyonnet, JG Morfín, FI Olness, JF Owens, I Schienbein, et al. ncteq15: Global analysis of nuclear parton distributions with uncertainties in the cteq framework. *Physical Review D*, 93(8):085037, 2016.